ARCHIVIO ISTITUZIONALE DELLA RICERCA

Alma Mater Studiorum Università di Bologna
Archivio istituzionale della ricerca

Accurate Analysis of Weighted Centroid Localization

This is the final peer-reviewed author's accepted manuscript (postprint) of the following publication:

Published Version:
Accurate Analysis of Weighted Centroid Localization / Kagiso Magowe ; Andrea Giorgetti ; Sithamparanathan Kandeepan ; Xinghuo Yu. - In: IEEE TRANSACTIONS ON COGNITIVE COMMUNICATIONS AND NETWORKING. - ISSN 2332-7731. - ELETTRONICO. - 5:1(2019), pp. 153-164. [10.1109/TCCN.2018.2874452]

Availability:
This version is available at: https://hdl.handle.net/11585/674501 since: 2019-09-19

Published:

DOI: http://doi.org/10.1109/TCCN.2018.2874452

Terms of use:

Some rights reserved. The terms and conditions for the reuse of this version of the manuscript are specified in the publishing policy. For all terms of use and more information see the publisher's website.

This item was downloaded from IRIS Università di Bologna (https://cris.unibo.it/).
When citing, please refer to the published version.

(Article begins on next page)

20 April 2024

This is the post peer-review accepted manuscript of:

K. Magowe, A. Giorgetti, K. Sithamparanathan, and X. Yu, "Accurate Analysis of Weighted Centroid Localization," IEEE Trans. on Cognitive Comm. and Networking, 2018.

The published version is available online at:

http://dx.doi.org/10.1109/TCCN.2018.2874452

© 2018 IEEE. Personal use of this material is permitted. Permission from IEEE must be obtained for all other uses, in any current or future media, including reprinting/republishing this material for advertising or promotional purposes, creating new collective works, for resale or redistribution to servers or lists, or reuse of any copyrighted component of this work in other works.

Accurate Analysis of Weighted Centroid Localization

Kagiso Magowe, *Member, IEEE,* Andrea Giorgetti, *Senior Member, IEEE,*
Sithamparanathan Kandeepan, *Senior Member, IEEE,* and Xinghuo Yu, *Fellow, IEEE*

***Abstract*—Source localization of primary users (PUs) is a spectrum awareness feature that can be very useful in enhancing the functionality of cognitive radios (CRs). When the cooperating CRs have limited information about the PU, weighted centroid localization (WCL) based on received signal strength (RSS) measurements represents an attractive low-complexity solution. This paper proposes a new analytical framework to accurately calculate the performance of WCL based on the statistical distribution of the ratio of two quadratic forms in normal variables. In particular, we derive an analytical expression for the root mean square error (RMSE) and an exact expression for the cumulative distribution function (CDF) of the two-dimensional location estimate. The proposed framework accounts for the presence of independent and identically distributed (i.i.d.) shadowing as well as correlated shadowing with distance-dependent intensity. The methodology is general enough to include the analysis of the one-dimensional error, which leads also to the evaluation of the bias of the position estimate. Numerical results confirm that the analytical framework is able to predict the performance of WCL capturing all the essential aspects of propagation as well as CR network spatial topology.**

***Index Terms*—Blind estimation, cognitive radio, cumulative distribution function, weighted centroid localization, performance analysis, root mean square error.**

I. Introduction

THE reliance on wireless radio communications has grown considerably in recent years, and the proliferation of wireless technology devices and user expectations place a burden on the already scarce radio spectrum. The radio spectrum is a finite natural resource which is traditionally managed by radio regulatory agencies and is allocated on a fixed spectrum assignment policy [3]. This allocation policy exacerbates the spectrum scarcity problem. As such, the wireless communication area has seen the introduction of new paradigms that aim to combat the issue of radio frequency spectrum scarcity. Cognitive radio (CR) is one of the emerging technologies that has been developed and studied over the past decade to enable efficient utilization of the spectrum resources [4]–[6]. In CR networks, spectrum sensing is a key enabler in identifying spectrum holes and monitoring of the primary user (PU) activity so as to avoid any potential harmful interference [7]–[10].

However, it should be noted that sensing functionality includes any kind of technique that allows the CRs to gather useful radio environment information and enhance the functionality of the network. Therefore, geo-location of PU is one such spectrum awareness technique that not only plays an important role in preventing harmful interference to the incumbent spectrum users, but allows for better spectrum resource allocations in the spatial domain [11]–[27]. It is worth noting that most of the aforementioned work has predominantly focused on a single PU scenario, with very limited work investigating the multiple PU localization problem [28], [29]. The accessibility of geo-location information is not only crucial for CR networks but essential for other emerging next generation wireless applications e.g, automotive radar technology, Internet of things, in-vehicle connected devices and MIMO radar systems [19], [30]–[38]. Since many of these systems are usually equipped with small low-cost, low-powered sensors, it is often of utter importance to develop localization algorithms that are very simple and scalable e.g., [39], [40]. Additionally, in the presence of nodes mobility e.g., connected devices (sensors) in cars, it is often of interest to keep track of those devices [33], [41]. However, the actual position of sensors can be affected by errors due to imperfect knowledge as well as delays in the position update. This imperfection should be noted as it can be detrimental to the accuracy of the localization algorithm.

Bearing in mind the challenges posed by the uncooperative (blind) nature of the PU in CR networks, weighted centroid localization (WCL) represents an attractive low complexity solution which can rely only on, e.g., received signal strength (RSS) measurements.[1] It should be noted that localization of non-cooperative PU is not limited only to RSS measurements, but other measurements such as direction of arrival (DoA) and time difference of arrival (TDoA) can also be adopted [42]–[44]. However, the drawback of TDoA and DoA approaches is that they are computationally expensive techniques [5], [45]. The WCL technique has been investigated in several papers assuming the secondary users (SUs) have limited information about the PU [45]–[59]. The original coarse-grained centroid

This work was presented in part at the European Signal Processing Conf. (EUSIPCO 2016), Budapest, Hungary, Aug. 2016 [1] and Int. Conf. on Commun. (ICC 2017), Paris, France, May 2017 [2].

This work was supported in part by the European Project eCircular (EIT Climate-KIC) and the Australian Government Research Training Program Scholarship.

K. Magowe, S. Kandeepan, and X. Yu are with the School of Engineering, RMIT University, Melbourne VIC 3001, Australia (e-mail: {kagiso.magowe.au, kandeepan}@ieee.org, x.yu@rmit.edu.au).

A. Giorgetti is with the Department of Electrical, Electronic, and Information Engineering "Guglielmo Marconi," University of Bologna, Cesena 47522, Italy (e-mail: andrea.giorgetti@unibo.it).

[1]The term *blind* captures the notion that location estimate is performed without any knowledge of the PU transmitted waveform. In particular, the cooperating receivers (SUs) have limited knowledge about the PU, and such blind estimators determine the location of the emitter with the only available data.

localization algorithm used to estimate the position of a transmitter using only the coordinates of the receiving devices in an outdoor environment was studied in [46]. An indoor localization with a low complexity weighted centroid approach combined with signal strength measurements was analyzed in [47]. In [48], WCL algorithm in outdoor sensor networks was proposed, where the link quality indicator has been used as weight. The work in [49] extends the result presented in [48] and the considered WCL algorithm with normalized values of the link quality indicator. Relative span weighted localization and relative span exponential weighted localization (REWL) mechanisms, which assign linear weights and exponential weights, respectively, were introduced in [50]. In [51], the authors adopted WCL in conjunction with the estimation of the path-loss exponent. The work in [52] characterized the indoor propagation channel, and further analyzed the accuracy of WCL and REWL algorithms. Several work adopted WCL under different network scenarios including distributed implementation, node selection, geometric constraints and clustering [45], [53]–[57].

Most of the aforementioned existing works evaluate the WCL performance only numerically, in terms of the root mean square error (RMSE), under varying environment conditions, i.e., factors such as node placement, node density, shadowing variance and node spacing. The fundamental theoretical framework for WCL analysis was presented in [53], assuming that the two-dimensional localization errors are jointly Gaussian. In particular, the authors derived analytical expressions for the error distribution of WCL in the presence of shadowing. A very promising extension of WCL with the adoption of cyclic autocorrelation of the received signals as weights to robustify WCL under the presence of interference have been proposed very recently in [59]. In the same work, the authors provide the analysis of the RMSE degradation due to co-channel interference.

In this work, we put forth a new analytical framework to calculate the exact performance of WCL in the presence of independent and identically distributed (i.i.d.) as well as correlated log-normal shadowing, based on results on the ratio of two quadratic forms in normal random variables (r.v.) [59]–[62]. To the best of our knowledge, the characterization of the performance of WCL in terms of the cumulative distribution function (CDF) has not been investigated before. The main contributions of this paper can be summarized as follows:

- We propose a general analytical expression for the RMSE of the two-dimensional location estimation.
- We derive the expression for the CDF of the error of the two-dimensional location estimation.
- We provide an expression for the bias of the localization error based on the fractional moment of the one-dimensional location estimate. Based on this, we prove that WCL estimation is bias dominated.
- The exact expressions are based on the statistical distribution of the ratio of quadratic forms in normal variables and apply for arbitrary covariance matrices, accommodating also distance-dependent shadowing intensity.
- We propose a coarse but very simple RMSE formula that considers only the mean received signal strength which provides fairly accurate performance estimation in weakly shadowed scenarios.

TABLE I
NOTATIONS AND SYMBOLS

$\mathbf{X}$	Matrix
$\mathbf{x}$	Vector
$\mathbb{E}[\cdot]$	Expectation operator
$\mathbb{V}[\cdot]$	Variance operator
$\mathrm{Tr}(\cdot)$	Trace operator
$\det(\cdot)$	Determinant of a matrix
$\mathrm{diag}(\cdot)$	Diagonal matrix
$\mathbf{I}$	Identity matrix
$\mathbf{1}$	Matrix of ones
$\mathbf{i}$	Column vector of ones
$[\cdot]^{\mathrm{T}}$	Transpose operator
$\|\cdot\|_l$	l-th norm operator
$\chi^2(a)$	Noncentral chi-squared distribution with one degree of freedom and noncentral parameter a
$\mathcal{N}(\boldsymbol{\mu}, \boldsymbol{\Sigma})$	Multivariate Gaussian distribution with mean $\boldsymbol{\mu}$ and covariance $\boldsymbol{\Sigma}$

The remainder of this paper is organized as follows. In Section II we present the system model. The derivation of the analytical expression for the RMSE is provided in Section III. In Section IV we derive the CDF of the estimation error. We analyze a case study to quantify the effectiveness of the proposed approach in Section V. Section VI concludes the paper. For the sake of conciseness, Table I summarizes the notations and symbols used. Throughout this paper, the terms slow-fading and shadow fading will be used interchangeably.

II. System Model

We consider a CR network with N SUs at positions $\boldsymbol{\ell}_i = [x_i, y_i]^{\mathrm{T}}$, with $i = 1, ..., N$, and a PU at position $\boldsymbol{\ell}_{\mathrm{p}} = [x_{\mathrm{p}}, y_{\mathrm{p}}]^{\mathrm{T}}$. The propagation environment is characterized by a distance-dependent path-loss channel model and log-normal shadowing. Thus, the RSS (in dBm) at the i-th SU node from the PU is given by

$$p_i = P_{\mathrm{T}} - \mathsf{PL}\left(\|\boldsymbol{\ell}_i - \boldsymbol{\ell}_{\mathrm{p}}\|_2\right) + s_i \tag{1}$$

where P_{T} is the transmit power in dBm, $\mathsf{PL}(d)$ is the path-loss (in dB) at a distance d, and s_i describes the random shadowing effect. More precisely, in the general case of correlated shadowing, $\mathbf{s} = [s_1, \ldots, s_N]^{\mathrm{T}} \sim \mathcal{N}(\mathbf{0}, \boldsymbol{\Sigma}_{\mathrm{s}})$ where $\boldsymbol{\Sigma}_{\mathrm{s}}$ is the shadowing covariance matrix. In case of independent shadowing among sensors $\boldsymbol{\Sigma}_{\mathrm{s}} = \mathrm{diag}\left(\sigma^2_{\mathrm{s},1}, \ldots, \sigma^2_{\mathrm{s},N}\right)$, which further simplifies in the i.i.d. case, i.e., $\boldsymbol{\Sigma}_{\mathrm{s}} = \sigma^2_{\mathrm{s}}\mathbf{I}$.[2]

We begin by presenting the WCL algorithm used to estimate the location of the PU in two dimensions [48]

$$\widehat{\boldsymbol{\ell}}_{\mathrm{p}} = \frac{\sum_{i=1}^{N} w_i \boldsymbol{\ell}_i}{\sum_{i=1}^{N} w_i} = \frac{\sum_{i=1}^{N} (p_i - P_{\min})\boldsymbol{\ell}_i}{\sum_{i=1}^{N} (p_i - P_{\min})} \tag{2}$$

[2]Note that, both the correlated shadowing case and the independent shadowing case, can accommodate a distance-dependent shadowing intensity, i.e., the diagonal elements of $\boldsymbol{\Sigma}_{\mathrm{s}}$ can be unequal (see Section V).

where $w_i = (p_i - P_{\min})/(P_{\max} - P_{\min})$ is the weighting coefficient for the i-th SU node, with $P_{\max}$ the maximum received power among sensor nodes, and $P_{\min}$ an arbitrary reference power level which can be e.g., the minimum measurable received power by the SU.[3]

The localization error is defined as $\boldsymbol{\xi} \triangleq \widehat{\boldsymbol{\ell}}_{\rm p} - \boldsymbol{\ell}_{\rm p} = [\widehat{x}_{\rm p} - x_{\rm p}, \widehat{y}_{\rm p} - y_{\rm p}]^{\rm T}$, where $\widehat{x}_{\rm p}$ and $\widehat{y}_{\rm p}$ are the one-dimensional position estimates along the x-axis and y-axis, respectively

$$\widehat{x}_{\rm p} = \frac{\sum_{i=1}^{N} g_i x_i}{\sum_{i=1}^{N} g_i} \qquad \widehat{y}_{\rm p} = \frac{\sum_{j=1}^{N} g_j y_j}{\sum_{j=1}^{N} g_j} \tag{3}$$

with $g_i = p_i - P_{\min}$. Finally, the distance error under the l_2-norm is given by

$$\xi \triangleq \sqrt{(\widehat{x}_{\rm p} - x_{\rm p})^2 + (\widehat{y}_{\rm p} - y_{\rm p})^2} = \|\boldsymbol{\xi}\|_2. \tag{4}$$

For notational convenience we define $\mathbf{g} = [g_1, \ldots, g_N]^{\rm T}$, $\mathbf{x} = [x_1, \ldots, x_N]^{\rm T}$, and $\mathbf{y} = [y_1, \ldots, y_N]^{\rm T}$. Note that $\mathbf{g} \sim \mathcal{N}(\boldsymbol{\mu}, \boldsymbol{\Sigma}_{\rm s})$, with $\boldsymbol{\mu} = \mathbb{E}[\mathbf{g}]$, i.e., $\boldsymbol{\mu} = [\mu_1, \ldots, \mu_N]^{\rm T}$ with $\mu_i = \mathbb{E}[g_i] = \mathbb{E}[p_i] - P_{\min}$.

In the following section, the square of the distance error (4) will be interpreted as the ratio of two quadratic forms, leading to a new theoretical framework for the performance analysis of WCL.

III. Calculation of the Root Mean Square Error

In this section we derive an accurate expression of the RMSE of the two-dimensional location estimate in the general setting with correlated shadowing, and we then provide an analytical expression for the RMSE in the i.i.d. case. We analyze the bias and the one-dimensional error, and we also propose a simplified RMSE predictor which can provide fairly accurate results in scenarios characterized by weak shadowing.

Defining $\xi_{\rm x} = \widehat{x}_{\rm p} - x_{\rm p}$ and $\xi_{\rm y} = \widehat{y}_{\rm p} - y_{\rm p}$ as the errors in the x-dimension and y-dimension, respectively, the RMSE can be written as

$$\mathsf{RMSE} = \sqrt{\mathbb{E}\left[\left\|\widehat{\boldsymbol{\ell}}_{\rm p} - \boldsymbol{\ell}_{\rm p}\right\|_2^2\right]} = \sqrt{\mathbb{E}\left[\xi_{\rm x}^2 + \xi_{\rm y}^2\right]}. \tag{5}$$

The argument of the expectation in (5) can be rewritten as

$$\begin{aligned}\xi^2 &= \xi_{\rm x}^2 + \xi_{\rm y}^2 \\ &= \left(\frac{\sum_{i=1}^{N} g_i (x_i - x_{\rm p})}{\sum_{i=1}^{N} g_i}\right)^2 + \left(\frac{\sum_{j=1}^{N} g_j (y_j - y_{\rm p})}{\sum_{j=1}^{N} g_j}\right)^2 \\ &= \frac{\sum_{i=1}^{N}\sum_{j=1}^{N} g_i g_j a_{ij}}{\sum_{i=1}^{N}\sum_{j=1}^{N} g_i g_j}\end{aligned} \tag{6}$$

where $a_{ij} = (x_i - x_{\rm p})(x_j - x_{\rm p}) + (y_i - y_{\rm p})(y_j - y_{\rm p})$. Defining $x_i' = x_i - x_{\rm p}$ and $y_i' = y_i - y_{\rm p}$, the term a_{ij} can be expressed as $a_{ij} = x_i' x_j' + y_i' y_j'$, and arranged in a matrix form $\mathbf{A} = [a_{i,j}]_{i,j=1,\ldots,N}$ with $\mathbf{A} = \mathbf{x}'\mathbf{x}'^{\rm T} + \mathbf{y}'\mathbf{y}'^{\rm T}$, $\mathbf{x}' = [x_1', x_2', \ldots, x_N']^{\rm T}$, and $\mathbf{y}' = [y_1', y_2', \ldots, y_N']^{\rm T}$. It should be noted that $\mathbf{A}$ is symmetric. Therefore, using matrix-vector notation we obtain the following compact form of the squared error

$$\xi^2 = \frac{\mathbf{g}^{\rm T}\mathbf{A}\mathbf{g}}{\mathbf{g}^{\rm T}\mathbf{B}\mathbf{g}} \tag{7}$$

where $\mathbf{B} = \mathbf{1}$ is the all-ones matrix, from which the mean square error (MSE) simply follows

$$\mathsf{MSE} = \mathbb{E}\left[\frac{\mathbf{g}^{\rm T}\mathbf{A}\mathbf{g}}{\mathbf{g}^{\rm T}\mathbf{B}\mathbf{g}}\right]. \tag{8}$$

Note that the expression (8) is the first order moment of the ratio of quadratic forms in normal variables, extensively investigated in [60], [61], [63]. According to the second condition in [61, Proposition 1], when the matrix $\mathbf{B}$ is not positive definite, the first order moment of (8) does not exist. Unfortunately, in our case the matrix $\mathbf{1}$ is positive semi-definite and nullifies the existence of (8). To obtain a finite value of the MSE in (8) we propose a weak perturbation of the matrix $\mathbf{1}$ which consists of adding a small constant $\epsilon > 0$ to its diagonal elements, i.e., we substitute $\mathbf{B} = \mathbf{1}$ with the matrix $\mathbf{B} = \mathbf{1}_\epsilon \triangleq \mathbf{I} \cdot \epsilon + \mathbf{1}$. With this approach now the matrix $\mathbf{B}$ is positive definite and we can proceed to calculate the first order moment. It is important to remark that the choice of ϵ is far from being critical. In scenarios of practical interest, values of ϵ in the range $10^{-5} - 10^{-1}$ provide almost coincident numerical results, confirming the robustness of this approach.[4] Moreover, as it will be explained in Section V, this approach predicts the RMSE with very high accuracy matching perfectly Monte-Carlo simulations.

In [61] it is possible to find the exact expression of expectation in the form of (8) when $\mathbf{g}$ is a vector of i.i.d. Gaussian r.v.'s with unit variance. More precisely,

$$\mathbb{E}\left[\frac{\mathbf{g}^{\rm T}\mathbf{A}\mathbf{g}}{\mathbf{g}^{\rm T}\mathbf{B}\mathbf{g}}\right] = \int_0^\infty \phi(0, -t)\left(\mathrm{Tr}(\mathbf{R}) + \tilde{\boldsymbol{\mu}}^{\rm T}\mathbf{R}\tilde{\boldsymbol{\mu}}\right) dt \tag{9}$$

where

$$\begin{aligned}\phi(0, -t) = &\left[\det(\mathbf{I} + 2t\mathbf{B})\right]^{-1/2} \\ &\times \exp\left(\frac{1}{2}\left(\boldsymbol{\mu}^{\rm T}(\mathbf{I} + 2t\mathbf{B})^{-1}\boldsymbol{\mu} - \boldsymbol{\mu}^{\rm T}\boldsymbol{\mu}\right)\right)\end{aligned} \tag{10}$$

is the joint moment generating function (MGF) of the ratio terms, t is the nuisance parameter, $\mathbf{R} = \mathbf{L}^{\rm T}\mathbf{A}\mathbf{L}$, $\tilde{\boldsymbol{\mu}} = \mathbf{L}^{\rm T}\boldsymbol{\mu}$, and $\mathbf{C}(t) = \mathbf{L}\mathbf{L}^{\rm T} = (\mathbf{I} + 2t\mathbf{B})^{-1}$.

A. Non–i.i.d. shadowing: correlated and distance-dependent slow-fading

[3] In general, $P_{\min}$ has to be chosen such that $p_i - P_{\min}$ is positive with very high probability. In fact, a negative weight, w_i, is equivalent to flipping the i-th SU position from $\boldsymbol{\ell}_i$ to $-\boldsymbol{\ell}_i$, degrading estimation performance.

[4] Regarding the choice of ϵ, we performed an extensive comparison between Monte-Carlo simulations and the analytical approach to assess the lack of any signicant discrepancy (less than 1%) over a broad range of values of ϵ that cover 4-order of magnitudes, i.e., from 10^{-5} to 10^{-1}.

To calculate the RMSE in a general setting we first extend (9) to encompass the non-i.i.d. case, $\mathbf{g} \sim \mathcal{N}(\boldsymbol{\mu}, \boldsymbol{\Sigma}_{\mathrm{s}})$, through the following transformation

$$\mathbf{g}^{\mathrm{T}}\mathbf{A}\mathbf{g} = \breve{\mathbf{g}}^{\mathrm{T}} \underbrace{\mathbf{V}\mathbf{A}\mathbf{V}}_{\triangleq \breve{\mathbf{A}}} \breve{\mathbf{g}} \qquad \mathbf{g}^{\mathrm{T}}\mathbf{B}\mathbf{g} = \breve{\mathbf{g}}^{\mathrm{T}} \underbrace{\mathbf{V}\mathbf{B}\mathbf{V}}_{\triangleq \breve{\mathbf{B}}} \breve{\mathbf{g}}$$

where $\mathbf{V} = {\boldsymbol{\Sigma}_{\mathrm{s}}}^{1/2}$ and $\breve{\mathbf{g}} \sim \mathcal{N}(\mathbf{V}^{-1}\boldsymbol{\mu}, \mathbf{I})$. Therefore, the non-i.i.d. scenario can be analyzed by applying (9) to

$$\mathsf{MSE} = \mathbb{E}\left[\frac{\breve{\mathbf{g}}^{\mathrm{T}}\breve{\mathbf{A}}\breve{\mathbf{g}}}{\breve{\mathbf{g}}^{\mathrm{T}}\breve{\mathbf{B}}\breve{\mathbf{g}}}\right]. \tag{11}$$

In this case, $\mathbf{C}(t) = \mathbf{L}\mathbf{L}^{\mathrm{T}} = (\mathbf{I} + 2t\breve{\mathbf{B}})^{-1}$ and $\tilde{\boldsymbol{\mu}} = \mathbf{L}^{\mathrm{T}}\mathbf{V}^{-1}\boldsymbol{\mu}$, so the terms within the integral (10) becomes, respectively

$$\mathrm{Tr}(\mathbf{R}) = \mathrm{Tr}(\mathbf{L}^{\mathrm{T}}\breve{\mathbf{A}}\mathbf{L}) = \mathrm{Tr}(\breve{\mathbf{A}}\mathbf{L}\mathbf{L}^{\mathrm{T}}) = \mathrm{Tr}(\breve{\mathbf{A}}\mathbf{C}(t))$$

and

$$\begin{aligned}\tilde{\boldsymbol{\mu}}^{\mathrm{T}}\mathbf{R}\tilde{\boldsymbol{\mu}} &= \boldsymbol{\mu}^{\mathrm{T}}\mathbf{V}^{-1}\mathbf{L}\mathbf{R}\mathbf{L}^{\mathrm{T}}\mathbf{V}^{-1}\boldsymbol{\mu} = \boldsymbol{\mu}^{\mathrm{T}}\mathbf{V}^{-1}\mathbf{L}\mathbf{L}^{\mathrm{T}}\breve{\mathbf{A}}\mathbf{L}\mathbf{L}^{\mathrm{T}}\mathbf{V}^{-1}\boldsymbol{\mu} \\ &= \boldsymbol{\mu}^{\mathrm{T}}\mathbf{V}^{-1}\mathbf{C}(t)\breve{\mathbf{A}}\mathbf{C}(t)\mathbf{V}^{-1}\boldsymbol{\mu}\end{aligned}$$

leading to the expression of the form

$$\mathrm{Tr}(\mathbf{R}) + \tilde{\boldsymbol{\mu}}^{\mathrm{T}}\mathbf{R}\tilde{\boldsymbol{\mu}} = \mathrm{Tr}(\breve{\mathbf{A}}\mathbf{C}(t)) + \boldsymbol{\mu}^{\mathrm{T}}\mathbf{V}^{-1}\mathbf{C}(t)\breve{\mathbf{A}}\mathbf{C}(t)\mathbf{V}^{-1}\boldsymbol{\mu}. \tag{14}$$

Noting that in our setting

$$\det(\mathbf{I} + 2t\breve{\mathbf{B}}) = \prod_{j=1}^{N}(1 + 2t\breve{b}_j)$$

where $\breve{b}_1, ..., \breve{b}_N$ are the eigenvalues of matrix $\breve{\mathbf{B}}$, the joint MGF in (10) becomes

$$\begin{aligned}\phi(0, -t) = &\prod_{j=1}^{N}(1 + 2t\breve{b}_j)^{-1/2} \\ &\times \exp\left(\frac{\boldsymbol{\mu}^{\mathrm{T}}\mathbf{V}^{-1}\big(\mathbf{C}(t) - \mathbf{I}\big)\mathbf{V}^{-1}\boldsymbol{\mu}}{2}\right).\end{aligned} \tag{15}$$

Substituting (14) and (15) into (9) we obtain the desired expression for the MSE (12) and consequently the RMSE in (5). We again emphasize that in our setting, $\boldsymbol{\Sigma}_{\mathrm{s}}$ is a general covariance matrix i.e., it can either model correlated shadowing or independent shadowing with distance-dependent intensity.

B. Independent and identically distributed shadowing

The general expression (12) can be simplified in the i.i.d. shadowing scenario, where $\mathbf{g} \sim \mathcal{N}(\boldsymbol{\mu}, \sigma_{\mathrm{s}}^2\mathbf{I})$. In particular, $\mathbf{V} = \sigma_{\mathrm{s}}\mathbf{I}$ so $\breve{\mathbf{g}} \sim \mathcal{N}(\boldsymbol{\mu}/\sigma_{\mathrm{s}}, \mathbf{I})$, $\breve{\mathbf{A}} = \sigma_{\mathrm{s}}^2\mathbf{A}$ and $\breve{\mathbf{B}} = \sigma_{\mathrm{s}}^2\mathbf{B} = \sigma_{\mathrm{s}}^2\mathbf{1}_\epsilon$, hence the MSE can be simplified as

$$\mathsf{MSE} = \mathbb{E}\left[\frac{\breve{\mathbf{g}}^{\mathrm{T}}\breve{\mathbf{A}}\breve{\mathbf{g}}}{\breve{\mathbf{g}}^{\mathrm{T}}\breve{\mathbf{B}}\breve{\mathbf{g}}}\right] = \mathbb{E}\left[\frac{\breve{\mathbf{g}}^{\mathrm{T}}\mathbf{A}\breve{\mathbf{g}}}{\breve{\mathbf{g}}^{\mathrm{T}}\mathbf{1}_\epsilon\breve{\mathbf{g}}}\right]. \tag{16}$$

In this case, the matrix $\mathbf{C}(t) = \mathbf{L}\mathbf{L}^{\mathrm{T}} = (\mathbf{I} + 2t\mathbf{1}_\epsilon)^{-1}$ becomes

$$\mathbf{C}(t) = \big((1 + 2\epsilon t)\mathbf{I} + 2t\mathbf{1}\big)^{-1}$$

which in turn can be expressed in the form of Sherman-Morrison formula [64] as[5]

$$\mathbf{C}(t) = \phi(t)\big(\mathbf{I} - \psi(t)\mathbf{1}\big) \tag{17}$$

with

$$\begin{aligned}\phi(t) &= \frac{1}{1 + 2\epsilon t} \\ \psi(t) &= \frac{2t}{1 + 2(N + \epsilon)t} \cong \frac{2t}{1 + 2Nt}.\end{aligned} \tag{18}$$

Note that the last term has been obtained considering that ϵ is always negligible (at least more than one order of magnitude) with respect to N. Furthermore, using matrix operations to reduce $(\mathbf{C}(t))^{-1}$ into a triangular matrix, we obtain

$$\begin{aligned}\det(\mathbf{I} + 2t\mathbf{1}_\epsilon) &= (1 + 2\epsilon t)^{N-1}\big(1 + 2(N + \epsilon)t\big) \\ &= \frac{2t}{\phi(t)^{N-1}\psi(t)}.\end{aligned} \tag{19}$$

Therefore, the MGF (10) reduces to

$$\begin{aligned}\phi(0, -t) = &\sqrt{\frac{\phi(t)^{N-1}\psi(t)}{2t}} \\ &\times \exp\left(\frac{\phi(t) - 1}{2\sigma_{\mathrm{s}}^2}\boldsymbol{\mu}^{\mathrm{T}}\boldsymbol{\mu} - \frac{\phi(t)\psi(t)}{2\sigma_{\mathrm{s}}^2}\boldsymbol{\mu}^{\mathrm{T}}\mathbf{1}\boldsymbol{\mu}\right).\end{aligned} \tag{20}$$

After some algebraic manipulations and considering that $\tilde{\boldsymbol{\mu}} = \mathbf{L}^{\mathrm{T}}\boldsymbol{\mu}/\sigma_{\mathrm{s}}$, the second term within the integral (10) can be rewritten in an easy to handle form

$$\begin{aligned}\mathrm{Tr}(\mathbf{R}) + \tilde{\boldsymbol{\mu}}^{\mathrm{T}}\mathbf{R}\tilde{\boldsymbol{\mu}} = &\phi(t)\left(\mathrm{Tr}(\mathbf{A}) - \psi(t)\mathrm{Tr}(\mathbf{A}\mathbf{1})\right) + \frac{\phi(t)^2}{\sigma_{\mathrm{s}}^2} \\ &\times \left(\boldsymbol{\mu}^{\mathrm{T}}\mathbf{A}\boldsymbol{\mu} - 2\psi(t)\boldsymbol{\mu}^{\mathrm{T}}\mathbf{A}\mathbf{1}\boldsymbol{\mu} + \psi(t)^2\boldsymbol{\mu}^{\mathrm{T}}\mathbf{1}\mathbf{A}\mathbf{1}\boldsymbol{\mu}\right).\end{aligned} \tag{21}$$

Finally, substituting (20) and (21) into (9) we obtain a simplified expression for the MSE (13) for the i.i.d. shadowing case which does not require matrix inversion and eigenvalue decomposition. Note that for convenience, in (13) we reported the coefficients Υ_i, with $i = 1, ..., 7$, which are simple scalar constants.

C. Bias and one-dimensional localization error

While the two-dimensional error represents the most important performance metric, it is also interesting to decompose the error along the axes to better understand the behavior of WCL. In this case, it is possible to calculate the bias of the estimate

[5]The Sherman-Morrison formula states that

$$\left(\mathbf{D} + \mathbf{u}\mathbf{v}^{\mathrm{T}}\right)^{-1} = \frac{\mathbf{D}^{-1}\mathbf{u}\mathbf{v}^{\mathrm{T}}\mathbf{D}^{-1}}{1 + \mathbf{v}^{\mathrm{T}}\mathbf{D}^{-1}\mathbf{u}}$$

where $\mathbf{D}$ is an invertible square matrix, and $\mathbf{u}$, $\mathbf{v}$ are column vectors. In our setting $\mathbf{D} = (1 + 2\epsilon t)\mathbf{I}$, $\mathbf{u} = 2t\mathbf{v}$, and $\mathbf{v} = [1, 1, ..., 1]^{\mathrm{T}}$.

$$\mathsf{MSE} = \int_0^\infty \prod_{j=1}^{N} (1+2t\breve{b}_j)^{-1/2} \exp\left(\frac{\boldsymbol{\mu}^{\mathrm{T}}\mathbf{V}^{-1}\big(\mathbf{C}(t)-\mathbf{I}\big)\mathbf{V}^{-1}\boldsymbol{\mu}}{2}\right)\left[\mathrm{Tr}(\breve{\mathbf{A}}\mathbf{C}(t)) + \boldsymbol{\mu}^{\mathrm{T}}\mathbf{V}^{-1}\mathbf{C}(t)\breve{\mathbf{A}}\mathbf{C}(t)\mathbf{V}^{-1}\boldsymbol{\mu}\right]dt$$

Non i.i.d. case (12)

$$\mathsf{MSE} = \int_0^\infty \sqrt{\frac{\phi(t)^{N+1}\psi(t)}{2t}} \exp\left(\frac{\phi(t)-1}{2\sigma_{\mathrm{s}}^2}\Upsilon_1 - \frac{\phi(t)\psi(t)}{2\sigma_{\mathrm{s}}^2}\Upsilon_2\right)\left[\Upsilon_3 - \psi(t)\Upsilon_4 + \frac{\phi(t)}{\sigma_{\mathrm{s}}^2}\left(\Upsilon_5 - 2\psi(t)\Upsilon_6 + \psi^2(t)\Upsilon_7\right)\right]dt$$

with

$$\Upsilon_1 = \boldsymbol{\mu}^{\mathrm{T}}\boldsymbol{\mu},\ \ \Upsilon_2 = \boldsymbol{\mu}^{\mathrm{T}}\mathbf{1}\boldsymbol{\mu},\ \ \Upsilon_3 = \mathrm{Tr}(\mathbf{A}),\ \ \Upsilon_4 = \mathrm{Tr}(\mathbf{A1}),\ \ \Upsilon_5 = \boldsymbol{\mu}^{\mathrm{T}}\mathbf{A}\boldsymbol{\mu},\ \ \Upsilon_6 = \boldsymbol{\mu}^{\mathrm{T}}\mathbf{A1}\boldsymbol{\mu},\ \ \Upsilon_7 = \boldsymbol{\mu}^{\mathrm{T}}\mathbf{1A1}\boldsymbol{\mu}$$

i.i.d. case (13)

components, $\mathbb{E}[\xi_{\mathrm{x}}]$ and $\mathbb{E}[\xi_{\mathrm{y}}]$. In particular, for the x-axis (and similarly for the y-axis)

$$\mathbb{E}[\xi_{\mathrm{x}}] = \mathbb{E}\left[\frac{\breve{\mathbf{g}}^{\mathrm{T}}\breve{\mathbf{A}}_{\mathrm{x}}\dot{\mathbf{1}}}{\breve{\mathbf{g}}^{\mathrm{T}}\breve{\mathbf{B}}_{\mathrm{x}}\dot{\mathbf{1}}}\right] = \mathbb{E}\left[\frac{(\breve{\mathbf{g}}^{\mathrm{T}}\tilde{\mathbf{A}}\breve{\mathbf{g}})^{1/2}}{(\breve{\mathbf{g}}^{\mathrm{T}}\tilde{\mathbf{B}}\breve{\mathbf{g}})^{1/2}}\right] \tag{22}$$

where $\breve{\mathbf{A}}_{\mathrm{x}} = \mathbf{V}\mathrm{diag}(\mathbf{x}')\mathbf{V}$, $\dot{\mathbf{1}}$ is a column vector of ones, $\breve{\mathbf{B}}_{\mathrm{x}} = \mathbf{VIV} = \boldsymbol{\Sigma}_{\mathrm{s}}$, $\tilde{\mathbf{A}} = \mathbf{V}\mathbf{x}'\mathbf{x}'^{\mathrm{T}}\mathbf{V}$, $\tilde{\mathbf{B}} = \mathbf{V1}_{\epsilon}\mathbf{V}$ and $\breve{\mathbf{g}} \sim \mathcal{N}(\mathbf{V}^{-1}\boldsymbol{\mu}, \mathbf{I})$. Note that (22) is a fractional moment of the ratio of quadratic forms in normal variables, for which recently an efficient computational procedure readily available as Matlab code was found [61].

Similarly, we can also investigate the MSE of ξ_{x}, i.e.,

$$\mathbb{E}[\xi_{\mathrm{x}}^2] = \mathbb{E}\left[\frac{\breve{\mathbf{g}}^{\mathrm{T}}\tilde{\mathbf{A}}\breve{\mathbf{g}}}{\breve{\mathbf{g}}^{\mathrm{T}}\tilde{\mathbf{B}}\breve{\mathbf{g}}}\right] \tag{23}$$

and thereafter use (9) and (10). We remark that we can compute (23) for non-i.i.d. as well as i.i.d. shadowing using (12) and (13), respectively.

It is worth mentioning that knowing the bias (22) along the two directions, it is possible to decompose the MSE (23) into $\mathbb{E}[\xi_{\mathrm{x}}^2] = \mathbb{V}[\widehat{x}_{\mathrm{p}}] + \mathbb{E}[\xi_{\mathrm{x}}]^2$, and also the MSE of the two-dimensional estimate (8) in the form

$$\mathsf{MSE} = \mathbb{E}\left[\xi^2\right] = \underbrace{\mathbb{V}\big[\widehat{x}_{\mathrm{p}}\big] + \mathbb{V}\big[\widehat{y}_{\mathrm{p}}\big]}_{\text{variance}} + \underbrace{\mathbb{E}\big[\xi_{\mathrm{x}}\big]^2 + \mathbb{E}\big[\xi_{\mathrm{y}}\big]^2}_{\text{bias}}. \tag{24}$$

This decomposition allows to derive the variance of the estimate and to evaluate the bias-variance tradeoff.

D. Coarse RMSE predictor in weak shadowing regime

To complete the detailed analysis which leads to a very accurate performance assessment, it is interesting to note that a coarse prediction of the RMSE of WCL can be obtained by neglecting the effect of shadowing. Such rough approximation is justified by the fact that in some scenarios the expected value μ_i of the received power is usually greater than its standard deviation, $\sigma_{\mathrm{s},i}$, so it is reasonable, to some extent, to ignore the effect of slow-fading. In this case, we replace $\mathbf{g}$ with its mean $\boldsymbol{\mu}$, so from (8) the RMSE can be approximated as

$$\mathsf{RMSE}_{\text{coarse}} = \sqrt{\frac{\boldsymbol{\mu}^{\mathrm{T}}\mathbf{A}\boldsymbol{\mu}}{\boldsymbol{\mu}^{\mathrm{T}}\mathbf{1}\boldsymbol{\mu}}}. \tag{25}$$

The effectiveness of (25) will be assessed in Section V.

IV. Cumulative Distribution Function of the Localization Error

In this section we derive the CDF expression of the distance error ξ, and equivalently of the squared error (6), in the general correlated shadowing setting with $\mathbf{g} \sim \mathcal{N}(\boldsymbol{\mu}, \boldsymbol{\Sigma}_{\mathrm{s}})$.

The distribution function of ξ can be derived as follows [60]

$$\begin{aligned}\mathsf{F}(q_0) = \Pr[\xi \le q_0] &= \Pr[\xi^2 \le q_0^2] \\ &= \Pr\left[\frac{\mathbf{g}^{\mathrm{T}}\mathbf{A}\mathbf{g}}{\mathbf{g}^{\mathrm{T}}\mathbf{B}\mathbf{g}} \le q_0^2\right] \\ &= \Pr[\mathbf{g}^{\mathrm{T}}\mathbf{A}\mathbf{g} \le q_0^2\mathbf{g}^{\mathrm{T}}\mathbf{B}\mathbf{g}] \\ &= \Pr[\mathbf{g}^{\mathrm{T}}\mathbf{W}\mathbf{g} \le 0]\end{aligned} \tag{26}$$

where $\mathbf{W} = \mathbf{A} - q_0^2\mathbf{B}$. The expression (26) shows that the distribution of the ratio of quadratic forms reduces to the distribution of an indefinite quadratic form $\mathbf{g}^{\mathrm{T}}\mathbf{W}\mathbf{g}$, where $\mathbf{W}$ is an indefinite matrix. Since the covariance of $\mathbf{g}$ is $\boldsymbol{\Sigma}_{\mathrm{s}}$, we can also rewrite (26) as

$$\begin{aligned}\mathsf{F}(q_0) &= \Pr[\mathbf{g}^{\mathrm{T}}{\boldsymbol{\Sigma}_{\mathrm{s}}}^{-1/2}{\boldsymbol{\Sigma}_{\mathrm{s}}}^{1/2}\mathbf{W}{\boldsymbol{\Sigma}_{\mathrm{s}}}^{1/2}{\boldsymbol{\Sigma}_{\mathrm{s}}}^{-1/2}\mathbf{g} \le 0] \\ &= \Pr[\mathbf{g}^{\mathrm{T}}\mathbf{V}^{-1}\mathbf{P}\mathbf{P}^{\mathrm{T}}\mathbf{V}\mathbf{W}\mathbf{V}\mathbf{P}\mathbf{P}^{\mathrm{T}}\mathbf{V}^{-1}\mathbf{g} \le 0] \\ &= \Pr[\mathbf{z}^{\mathrm{T}}\boldsymbol{\Lambda}\mathbf{z} \le 0]\end{aligned} \tag{27}$$

where $\mathbf{V} = {\boldsymbol{\Sigma}_{\mathrm{s}}}^{1/2}$, $\mathbf{z} = \mathbf{P}^{\mathrm{T}}\mathbf{V}^{-1}\mathbf{g}$ and $\mathbf{P}$ is an orthogonal matrix formed by eigenvectors of $\mathbf{VWV}$ such that $\boldsymbol{\Lambda} = \mathbf{P}^{\mathrm{T}}\mathbf{VWVP}$ is a diagonal matrix whose entries are the eigenvalues $\lambda_1, ..., \lambda_N$ of $\mathbf{VWV}$. Note that, although not explicitly denoted, the eigenvalues λ_j and the eigenvectors contained in $\mathbf{P}$ depend on q_0.

Note now that $\mathbf{z} \sim \mathcal{N}(\boldsymbol{\mu}_z, \mathbf{I})$ with $\boldsymbol{\mu}_z = \mathbf{P}^{\mathrm{T}}\mathbf{V}^{-1}\boldsymbol{\mu}$, so (27) is simply

$$\mathsf{F}(q_0) = \Pr\left[\sum_{i=1}^{N}\lambda_i z_i^2 \le 0\right] \tag{28}$$

where $z_i^2 \sim \chi^2(\mu_{zi}^2)$ is a noncentral chi-squared distributed r.v. with one degree of freedom and noncentral parameter μ_{zi}^2.[6] A numerical integration representation of (28) was presented by Imhof [65], which is based on the Gil-Pelaez [66] inversion formula for the indefinite quadratic form,

$$\mathsf{F}(q_0) = \frac{1}{2} - \frac{1}{\pi}\int_0^\infty t^{-1}\Im\{\varphi(t)\}dt \tag{29}$$

where $\Im\{\cdot\}$ represents the imaginary part and

$$\varphi(t) = \left[\prod_{j=1}^{N}(1-2it\lambda_j)^{-1/2}\right]\exp\left(i\sum_{j=1}^{N}\frac{\mu_{zj}^2\lambda_j t}{1-2it\lambda_j}\right)$$

is the characteristic function (CF) of $\mathbf{z}^{\mathrm{T}}\mathbf{\Lambda}\mathbf{z}$. Alternatively, it has been shown in [65] that (29) can be written as

$$\mathsf{F}(q_0) = \frac{1}{2} - \frac{1}{\pi}\int_0^\infty \frac{\sin\theta(v)}{v\rho(v)}dv \tag{30}$$

where

$$\theta(v) = \frac{1}{2}\sum_{j=1}^{N} r_j\tan^{-1}(\lambda_j v) + \mu_{zj}^2\lambda_j v(1+\lambda_j^2 v^2)^{-1}$$

$$\rho(v) = \left[\prod_{j=1}^{N}(1+\lambda_j^2 v^2)^{r_j/4}\right]\exp\left(\frac{1}{2}\sum_{j=1}^{N}\frac{\mu_{zj}^2\lambda_j^2 v^2}{1+\lambda_j^2 v^2}\right)$$

and r_j's are the multiplicities of the nonzero distinct eigenvalues λ_j. We remark that both (29) and (30) are exact expressions, however, the latter does not involve the use of complex numbers.

We also remark that despite the non-existence of the moments of the two-dimensional error when $\mathbf{B}$ is positive semi-definite, the CDF of ξ^2 is always well defined, so there is no need for the perturbation of $\mathbf{B}$.

V. Case Study Analysis

In this section, we exploit the methodology provided in Section III and Section IV, respectively, to investigate the performance of WCL.[7] In particular we compare analytical and Monte-Carlo simulation results of the RMSE and CDF of location estimation in three different settings:

- RF-SU) random, but fixed, SU positions. In particular, we consider a single snapshot (realization) of SU positions.
- R-SU) random SU positions. In particular, a semi-analytical approach which combines our analytical expressions with Monte-Carlo simulation.
- RE-SU) random SU positions with location uncertainty/error. In this case we assume that the generic $i-$th SU position, $\boldsymbol{\ell}_i^{\mathrm{u}}$, is a Gaussian distributed random vector, i.e., $\boldsymbol{\ell}_i^{\mathrm{u}} \sim \mathcal{N}(\boldsymbol{\ell}_i, \sigma_{\mathrm{u}}^2\mathbf{I})$.

[6]Note that for the i.i.d shadowing case $\mathbf{z} \sim \mathcal{N}(\boldsymbol{\mu}_z = \mathbf{P}^{\mathrm{T}}\boldsymbol{\mu}/\sigma_{\mathrm{s}}, \mathbf{I})$, since $\mathbf{V}^{-1} = \mathbf{I}/\sigma_{\mathrm{s}}$.

[7]Note that we do not present the analysis of communication overhead in WCL in this work. Such analysis can be found in [53].

The case study scenario is a square area with side $\mathcal{S} = 100\,\mathrm{m}$. Fig. 1 depicts the considered randomly distributed SUs and the PU located in three different positions: $\boldsymbol{\ell}_{\mathrm{p}}^{\mathrm{A}} = (0\,\mathrm{m}, 0\,\mathrm{m})$, $\boldsymbol{\ell}_{\mathrm{p}}^{\mathrm{B}} = (20\,\mathrm{m}, 0\,\mathrm{m})$ and $\boldsymbol{\ell}_{\mathrm{p}}^{\mathrm{C}} = (30\,\mathrm{m}, 30\,\mathrm{m})$.

The propagation environment is characterized by a power-law path-loss channel model and log-normal shadowing, where the RSS at the i-th SU node is given by (1) with the path-loss expressed as

$$\mathsf{PL}(d) = p_0 + 10\,\alpha\log_{10}\left(\frac{d}{d_0}\right) \tag{31}$$

where $P_{\mathrm{T}} = 20\,\mathrm{dBW}$, $p_0 = 50\,\mathrm{dB}$ is the path-loss at a reference distance $d_0 = 1\,\mathrm{m}$, α is the path-loss exponent ranging between $\alpha = 3$ and 4. Unless otherwise specified, the shadowing parameter (or intensity) is $\sigma_{\mathrm{s}} = 4\,\mathrm{dB}$, $5.5\,\mathrm{dB}$ and $8\,\mathrm{dB}$. The considered standard deviations of the SU locations uncertainty are $\sigma_{\mathrm{u}} = 10\,\mathrm{m}$ and $\sigma_{\mathrm{u}} = 30\,\mathrm{m}$. As far as shadowing is concerned, we investigate three different situations:

- Correlated shadowing. We consider the following spatial correlation model [67]–[69]

  $$\mathbf{\Sigma}_{\mathrm{s}} = [\Sigma_{ij}]_{i,j=1,\ldots,N} \text{ with } \Sigma_{ij} = \sigma_{\mathrm{s}}^2 e^{-\beta\|\boldsymbol{\ell}_i - \boldsymbol{\ell}_j\|_2}$$

  where $\beta = 1/D_{\mathrm{c}}\,\mathrm{m}^{-1}$, and D_{c} is the correlation distance.
- Distance-dependent shadowing. In this case,

  $$\mathbf{\Sigma}_{\mathrm{s}} = \mathrm{diag}\left(\sigma_{\mathrm{s},1}^2, \ldots, \sigma_{\mathrm{s},N}^2\right)$$

  where the different shadowing parameters depend upon the distance according to the curve fitted model [70], i.e.,[8]

  $$\sigma_{\mathrm{s},i} = -3.08 + 7.69\log_{10}(\|\boldsymbol{\ell}_i - \boldsymbol{\ell}_{\mathrm{p}}\|_2). \tag{32}$$
- I.i.d. shadowing. In this case $\mathbf{\Sigma}_{\mathrm{s}} = \sigma_{\mathrm{s}}^2\mathbf{I}$.

To validate the analytical approach we used Monte-Carlo simulation with 10^6 runs. In particular, with the only exception of Fig. 8, in all figures lines and symbols refer to analytical and simulation results, respectively. The discussion of our numerical results will be based on the following effects: PU location, imperfect knowledge of SU positions, shadowing and path-loss. For the sake of clarity and completeness we will organize our numerical analysis as follows. The RMSE and CDF numerical results are discussed in Section V-A and Section V-B, respectively. Unless stated otherwise, the case study analysis will be based on the i.i.d. shadowing assumption.

Additionally, in the legends of figures, $\boldsymbol{\ell}_{\mathrm{p}}^{\mathrm{A}}(\beta)$, $\boldsymbol{\ell}_{\mathrm{p}}^{\mathrm{B}}(\beta)$, and $\boldsymbol{\ell}_{\mathrm{p}}^{\mathrm{C}}(\beta)$, denote correlated shadowing results, $\boldsymbol{\ell}_{\mathrm{p}}^{\mathrm{A}}(\sigma_{\mathrm{s},i})$, $\boldsymbol{\ell}_{\mathrm{p}}^{\mathrm{B}}(\sigma_{\mathrm{s},i})$, and $\boldsymbol{\ell}_{\mathrm{p}}^{\mathrm{C}}(\sigma_{\mathrm{s},i})$, refer to results for distance-dependent shadowing at the i-th SU, $\boldsymbol{\ell}_{\mathrm{p}}^{\mathrm{A}}(\sigma_{\mathrm{u}})$, $\boldsymbol{\ell}_{\mathrm{p}}^{\mathrm{B}}(\sigma_{\mathrm{u}})$, and $\boldsymbol{\ell}_{\mathrm{p}}^{\mathrm{C}}(\sigma_{\mathrm{u}})$, denote the SU location uncertainty scenarios for a given σ_{u}, $\boldsymbol{\ell}_{\mathrm{p}}^{\mathrm{A}}(\text{coarse})$, $\boldsymbol{\ell}_{\mathrm{p}}^{\mathrm{B}}(\text{coarse})$, and $\boldsymbol{\ell}_{\mathrm{p}}^{\mathrm{C}}(\text{coarse})$, refer to results for coarse RMSE predictors, when the PU is located at $\boldsymbol{\ell}_{\mathrm{p}}^{\mathrm{A}}$, $\boldsymbol{\ell}_{\mathrm{p}}^{\mathrm{B}}$, and $\boldsymbol{\ell}_{\mathrm{p}}^{\mathrm{C}}$, respectively.

A. RMSE Analyis

In this section, we quantify the performance of WCL in terms of the RMSE of position estimation in different

[8]To ensure that $\sigma_{\mathrm{s},i} > 0$, we fix a minimum distance below which (32) cannot decrease below 0 i.e., $\|\boldsymbol{\ell}_i - \boldsymbol{\ell}_{\mathrm{p}}\|_2 \geq 2.5$.

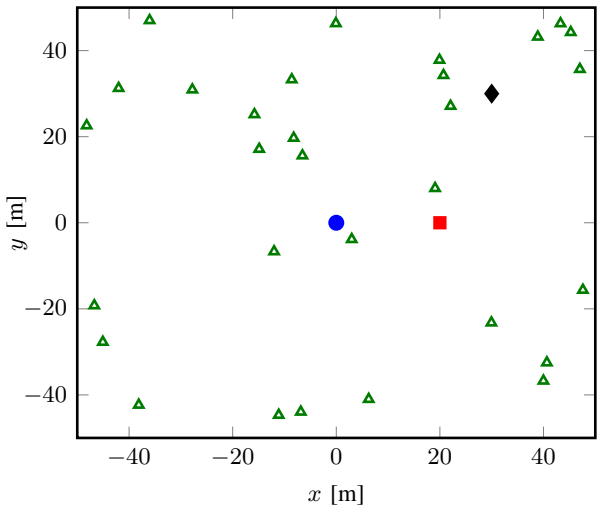

Fig. 1. The case study considered with randomly located SUs (triangles) and different PU positions: circle, square and diamond represent PU locations $\ell_{\mathrm{p}}^{\mathrm{A}}$, $\ell_{\mathrm{p}}^{\mathrm{B}}$ and $\ell_{\mathrm{p}}^{\mathrm{C}}$, respectively.

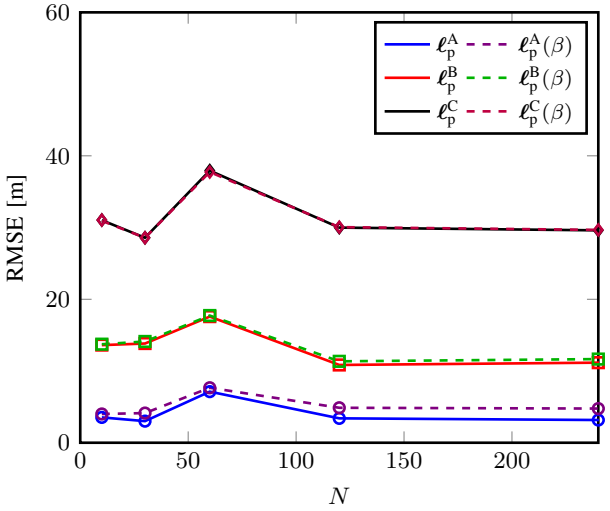

Fig. 2. RMSE of the two-dimensional position estimation as a function of the number of SU nodes, N, when the PU is located at $\ell_{\mathrm{p}}^{\mathrm{A}}$, $\ell_{\mathrm{p}}^{\mathrm{B}}$ and $\ell_{\mathrm{p}}^{\mathrm{C}}$. Dashed curves refer to correlated shadowing with $\beta = 1/30\,\mathrm{m}^{-1}$. Lines and symbols refer to analytical and simulation results, respectively.

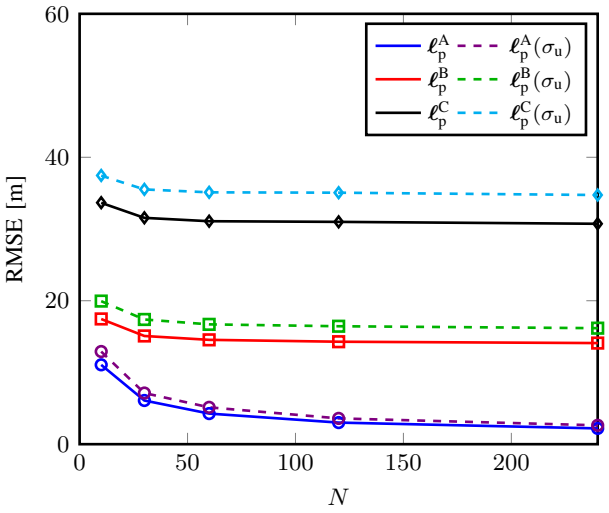

Fig. 3. RMSE of the two-dimensional position estimation as a function of the number of SU nodes, N, when the PU is located at $\ell_{\mathrm{p}}^{\mathrm{A}}$, $\ell_{\mathrm{p}}^{\mathrm{B}}$ and $\ell_{\mathrm{p}}^{\mathrm{C}}$. Dashed curves refer to the RE-SU case with $\sigma_{\mathrm{u}} = 30\,\mathrm{m}$. Lines and symbols refer to analytical and simulation results, respectively.

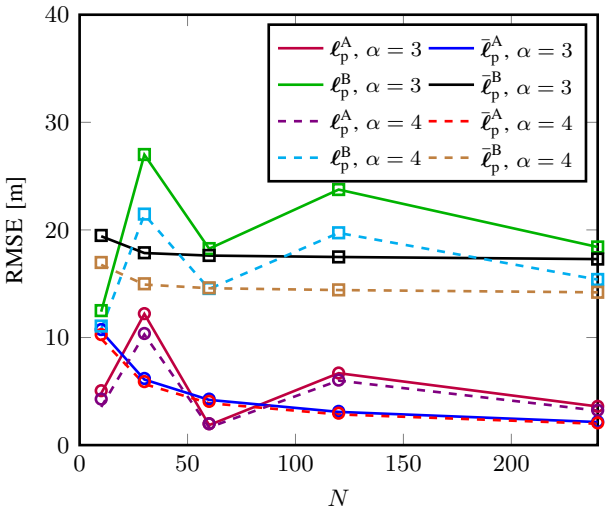

Fig. 4. RMSE of the two-dimensional position estimation as a function of the number of SU nodes, N, when the PU is located at $\ell_{\mathrm{p}}^{\mathrm{A}}$ and $\ell_{\mathrm{p}}^{\mathrm{B}}$, and for two different values of the path-loss exponent. The average RMSE in the R-SU case is denoted by $\bar{\ell}_{\mathrm{p}}^{\mathrm{A}}$ and $\bar{\ell}_{\mathrm{p}}^{\mathrm{B}}$. Lines and symbols refer to analytical and simulation results, respectively.

scenarios by varying the PU locations, the path-loss exponent, the shadowing standard deviation, the number of SUs and their location. Throughout this section, unless specified otherwise, the path-loss exponent and shadowing parameter are $\alpha = 4$ and $\sigma_{\mathrm{s}} = 8\,\mathrm{dB}$, respectively.

Impact of PU location and correlated shadowing. In Fig. 2 we depict the WCL performance for the i.i.d. and correlated shadowing scenarios using the analytical approach and Monte-Carlo simulation results in the RF-SU case for the aforementioned PU locations. As can be noticed, there is an increase in the RMSE as the PU moves from the center at $\ell_{\mathrm{p}}^{\mathrm{A}}$ towards the edge of the area at $\ell_{\mathrm{p}}^{\mathrm{C}}$. This behavior is due to the nature of WCL which tends to be biased towards the center of the network, as was also observed through numerical simulations in [45], [56]. It is also evident that for the PU locations $\ell_{\mathrm{p}}^{\mathrm{B}}$ and $\ell_{\mathrm{p}}^{\mathrm{C}}$, the WCL does not benefit from increasing the number of SUs and as a result the localization performance remains almost constant when N increases from 120 to 240. The fluctuation in the RMSE in a relatively low number of SUs regime is due to the specific nodes locations, chosen randomly, in which the geometric configuration among SUs relative to the PU impacts the RMSE. That is, the topology in Fig. 2 comprises a single realization of SU positions and in contrast to Fig. 3 we did not average over independent realizations of SU positions. This means that for e.g., $N = 20$ may result in favorable SU positions around the PU than say $N = 60$, and consequently leading to the non-monotonical behavior depicted in Fig. 2 , Fig. 4 and Fig. 7. However, averaging

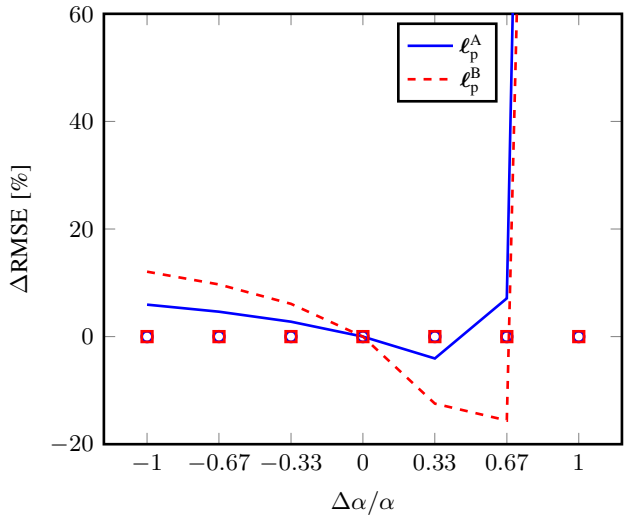

Fig. 5. Relative RMSE (ΔRMSE) of the two-dimensional position estimation as a function of the relative error in the path-loss exponent, $\Delta\alpha = \alpha' - \alpha$ where α is the true path-loss exponent and $\alpha' \in [0, 6]$ is the mismatch path-loss exponent, when the PU is located at ℓ_p^A and ℓ_p^B. Lines and symbols refer to analytical and simulation results, respectively. The numerical analysis was performed considering $N = 10$, and $\sigma_s = 6$ dB.

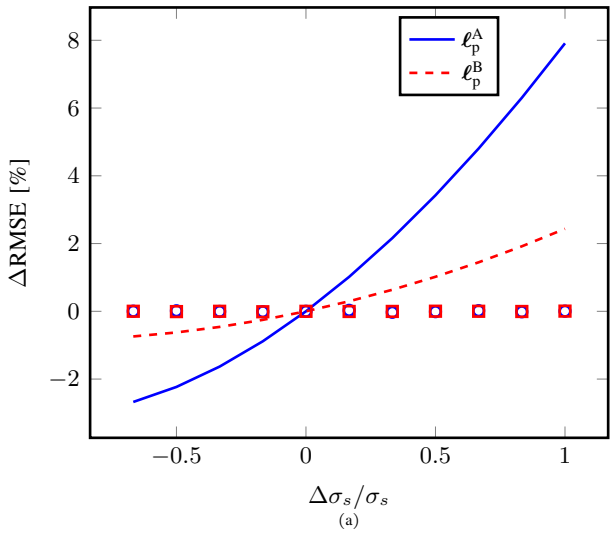

Fig. 6. Relative RMSE deviation (ΔRMSE) of the two-dimensional position estimation as a function of the relative error in the shadowing standard deviation, $\Delta\sigma_s = \sigma_s' - \sigma_s$ where σ_s is the shadowing standard deviation and $\sigma_s' \in [2, 12]$ is the mismatch shadowing standard deviation, when the PU is located at ℓ_p^A and ℓ_p^B. Lines and symbols refer to analytical and simulation results, respectively. The numerical analysis was performed considering $N = 10$, $\sigma_s = 6$ dB, and $\alpha = 3$.

over SU positions results in the error scaling monotically with N as shown in Fig. 3 and Fig. 4. It is also worth noting that Fig. 4 demonstrates both the non-monotonical behavior (no averaging) and the monotonical behavior (averaging).

When PU is in the center, correlation appears to degrade the performance of WCL. However, in other locations the impact of correlation seems to be minor mainly because the error is dominated by the WCL bias as demonstrated in Table II.

In Fig. 3 we illustrate the WCL performance using the averaged RMSE of the two-dimensional position estimation for the R-SU and RE-SU scenarios. The results are semi-analytical in the sense that we perform a Monte-Carlo simulation over (13) to obtain averaged results. It is now evident that, compared to Fig. 2 which uses only a single snapshot, the resulting Fig. 3 curves are smooth and as expected the performance improves with increasing N when the PU is at the center.

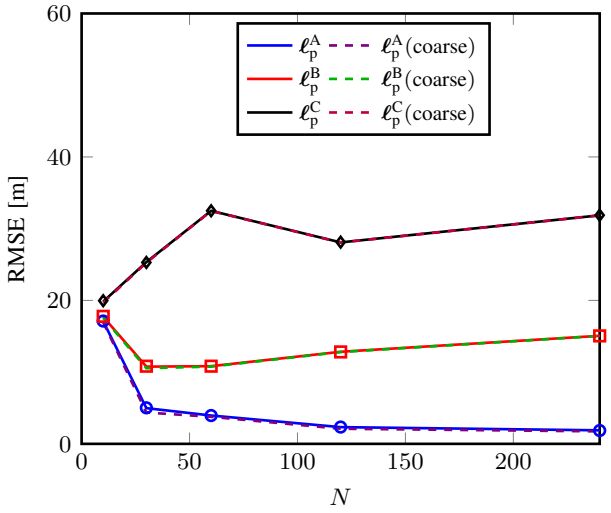

Fig. 7. RMSE of the two-dimensional position estimation as a function of the number of SU nodes, N, when the PU is located at ℓ_p^A, ℓ_p^B and ℓ_p^C. Dashed curves refer to RMSE calculated by the proposed coarse RMSE predictor. Lines and symbols refer to analytical and simulation results, respectively.

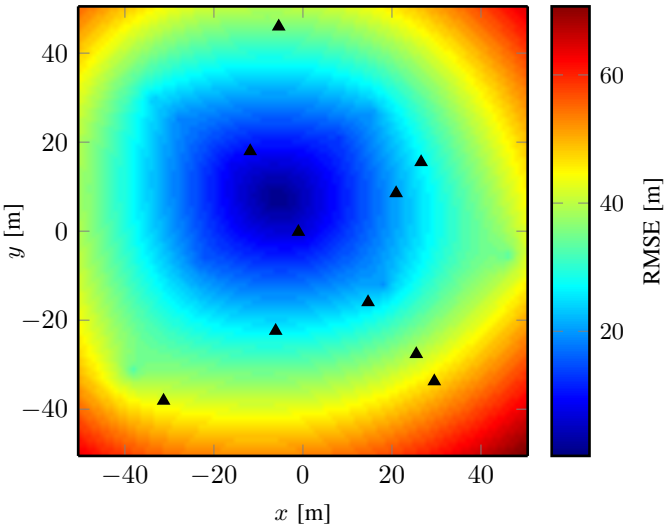

Fig. 8. RMSE of the two-dimensional position estimation for fixed number of SU nodes (black triangles), $N = 10$, and for different positions of the PU located within the square grid with equal spacing of 1 m.

Impact of uncertainty in SU locations. For the RE-SU scenario, we introduce uncertainty in the SU position with $\sigma_u = 30$ m. As shown in Fig. 3 this level of uncertainty degrades the performance of WCL and the impact is more noticable as the PU moves away from location ℓ_p^A. We expect the performance gap to widen for higher values of σ_u.

Path-loss Analysis. In Fig. 4 we show the impact the variation of the path-loss exponent α has on the RMSE, and

TABLE II
BIAS-VARIANCE TRADEOFF OF POSITION ESTIMATION WITH $N = 100$

PU ↓	MSE [m^2]	Bias [m^2]	Variance [m^2]	$\frac{\text{Bias}}{\text{MSE}}\%$
$\boldsymbol{\ell}_{\text{p}}^{\text{A}}$	15.9	9.94	5.96	62.7
$\boldsymbol{\ell}_{\text{p}}^{\text{B}}$	217.4	204.6	12.8	94.1
$\boldsymbol{\ell}_{\text{p}}^{\text{C}}$	818.7	792.8	25.9	96.8

we considered the following scenarios: PU locations $\boldsymbol{\ell}_{\text{p}}^{\text{A}}$ and $\boldsymbol{\ell}_{\text{p}}^{\text{B}}$, RF-SU and R-SU settings, $\alpha = 3$ and 4, $\sigma_{\text{s}} = 5.5\,\text{dB}$. Interestingly, the RMSE improves with an increase in α, as was observed numerically in [45]. Basically, increasing α in a way induces a node selection strategy which effectively reduces the impact of the SUs with low RSS on location estimate [45], [56]. This means that only SUs closer to the PU will contribute more in the localization and effectively improving the RMSE, especially when the PU is away from the center. We again remark that results in the RF-SU setting experience fluctuation in the WCL performance due to the impact of the specific node topology. However, in the R-SU case curves become smooth and consequently the accuracy of the WCL depends on the node density to some extent.

Effect of Parameter Mismatch. Fig. 5 and Fig. 6 provide results in the presence of mismatched channel model parameters e.g., shadowing standard deviation σ_s and path-loss exponent α between the simulation and our analytical tool. Fig. 5 depicts the ΔRMSE results as a function of the relative error in the path-loss exponent, $\Delta\alpha/\alpha$, where $\Delta\alpha = \alpha' - \alpha$ and α' is the mismatched path-loss exponent. Fig. 6 depicts the ΔRMSE results as a function of the relative error in the shadowing standard deviation, $\Delta\sigma_s/\sigma_s$, where $\Delta\sigma_s = \sigma_s' - \sigma_s$ and σ_s' is the mismatched σ_s. Fig. 5 clearly depicts the implications of overestimating ($\Delta\alpha > 0$) and underestimating ($\Delta\alpha < 0$) the path-loss exponent when using the analytical results. As a general rule, it is better to underestimate the path-loss exponent so as to avoid giving misleading and overly pessimistic or too optimistic results depending on $\Delta\alpha/\alpha$, according to the general rule that the design of the localization algorithm has to satisfy the worst-case scenario. For example, when the PU is in position $\boldsymbol{\ell}_{\text{p}}^{\text{A}}$, the role of α is less critical (though slightly optimistic for the latter) until the overestimation reaches the 67% mark above which it results in overly pessimistic RMSE values. Regarding the impact of a mismatched σ_s on the RMSE, Fig. 6 highlights the following behavior; when the PU is in position $\boldsymbol{\ell}_{\text{p}}^{\text{A}}$, for $\sigma_s' > \sigma_s$, the analytical approach overestimates the RMSE by up to 8% and for $\sigma_s' < \sigma_s$, the deviation from the true RMSE is less than 3%.[9] We observe a similar behavior when the PU is in position $\boldsymbol{\ell}_{\text{p}}^{\text{B}}$. Based on these observations, we can conclude that it is better to overestimate σ_s than to underestimate it so as to avoid presenting optimistic results.

Coarse RMSE predictor. The performance of the proposed simple estimator (25) is depicted in Fig. 7. Remarkably it provides a very good performance estimate as the analytical RMSE, which in a way further demonstrates the strong dependence of the RMSE on the mean path-loss than σ_{s} in weak shadowing regime.[10]

Bias-variance tradeoff. Table II shows the relationship between the MSE (12) and bias terms in (24) across all the three locations of interest with $N = 100$. The ratio of the bias to MSE expressed as a percentage clearly demonstrate that the WCL estimation is bias dominated, and this is even more apparent at locations $\boldsymbol{\ell}_{\text{p}}^{\text{B}}$ and $\boldsymbol{\ell}_{\text{p}}^{\text{C}}$ experiencing a position estimation where more than $90\,\%$ of the MSE is due to bias.

RMSE map. Fig. 8 depicts the WCL performance when considering the RF-SU scenario, with $N = 10$, and for varying positions of the PU on a regular grid within the area with spacing of $1\,\text{m}$. As expected, the WCL performance radially deteriorates as the PU moves away from the center of the area.

B. Localization Error Probability Analysis

In this section, we describe the performance of the WCL in terms of the CDF of the error, $\mathsf{F}(q_0) = \Pr[\xi \leq q_0]$, known as localization error probability (LEP). Fig. 9 – Fig. 12 summarize the CDF analysis when considering the RF-SU and R-SU positions.

Impact of PU location and correlated shadowing. In Fig. 9 we show the CDF using the exact analytical expression (29) and Monte-Carlo simulations, for different PU locations, $N = 50$ fixed SU positions, i.e., the RF-SU setting, $\alpha = 4$, and correlated shadowing with $\sigma_{\text{s}} = 8\,\text{dB}$ and $\beta = 1/30\,\text{m}^{-1}$, as well as distance-dependent shadowing with $\sigma_{\text{s},i}$ evaluated by (32). The curve that refers to PU position $\boldsymbol{\ell}_{\text{p}}^{\text{A}}$ reaches a high probability faster than the other curves, which confirms that the PU in the center is the most favorable situation.

We also investigated the effect of correlated shadowing and for PU at $\boldsymbol{\ell}_{\text{p}}^{\text{A}}$, the correlation degrades the performance (in accordance to the increase in the RMSE in Fig. 2). For PU at $\boldsymbol{\ell}_{\text{p}}^{\text{B}}$ and $\boldsymbol{\ell}_{\text{p}}^{\text{C}}$ the correlation makes the CDF less sharp. Hence, the performance is degraded and improved for high LEP and low LEP, respectively. It is usually interesting to look for high values of the LEP, e.g., $0.8 - 1$, and in this range correlation degrades the performance. Interestingly, for $q_0 = 15\,\text{m}$ and $q_0 = 32\,\text{m}$ the LEP is independent of shadowing distance for locations $\boldsymbol{\ell}_{\text{p}}^{\text{B}}$ and $\boldsymbol{\ell}_{\text{p}}^{\text{C}}$, respectively. It can also be observed that for all the three locations, distance-dependent shadowing have negligible impact on the performance.

In Fig. 10 we provide results for a scenario similar to the one considered in Fig. 9, except that now performances are averaged over R-SU positions, and we also introduce results for $N = 10$. The node density improves the performance of the WCL, especially for high LEPs. However, for PU locations $\boldsymbol{\ell}_{\text{p}}^{\text{B}}$ and $\boldsymbol{\ell}_{\text{p}}^{\text{C}}$ we observe a crossing point between LEP curves for $q_0 = 13\,\text{m}$ and $q_0 = 30\,\text{m}$, respectively.

Impact of uncertainty in SU locations. Fig. 11 depicts the performance of WCL for the R-SU scenario, when considering

[9]Note that since $\Delta\text{RMSE} = \frac{\text{mismatch RMSE - true RMSE}}{\text{true RMSE}}$, $\Delta\text{RMSE} > 0$ means that we are overestimating the error, and $\Delta\text{RMSE} < 0$ implies that we are underestimating the error.

[10]We performed numerical analysis demonstrating the RMSE deviation between the coarse method and the accurate method as a function of σ_s. For example, when considering $\sigma_s = 6\,\text{dB}$, the RMSE deviation between the coarse predictor and the accurate approach is about 5% and 0.2% for $\boldsymbol{\ell}_{\text{p}}^{\text{A}}$ and $\boldsymbol{\ell}_{\text{p}}^{\text{B}}$, respectively.

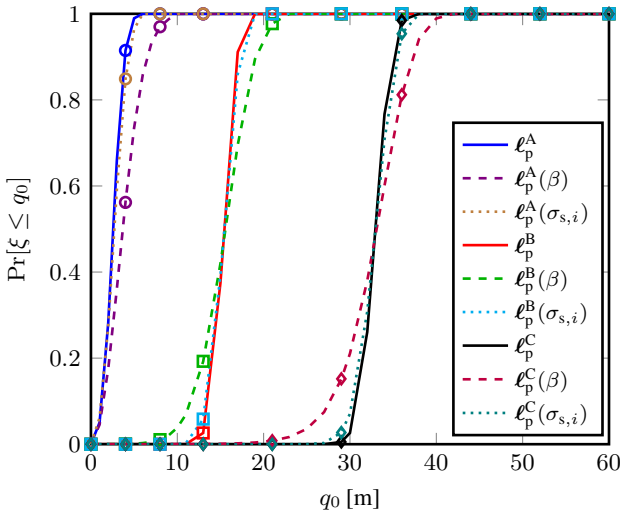

Fig. 9. CDF of the error of the two-dimensional position estimation when the PU is located at ℓ_p^A, ℓ_p^B and ℓ_p^C, for $N = 50$. Dashed lines refer to correlated shadowing with $\beta = 1/30\,\mathrm{m}^{-1}$, while dotted curves refer to distance-dependent shadowing. Lines and symbols refer to analytical and simulation results, respectively.

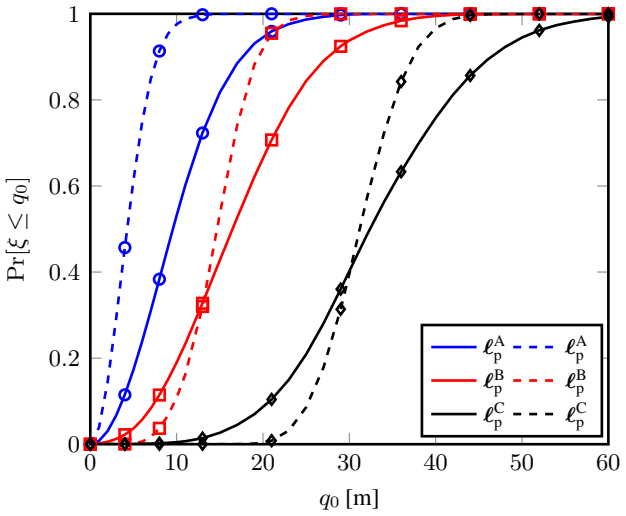

Fig. 10. CDF of the error of the two-dimensional position estimation, in the R-SU case, when the PU is located at ℓ_p^A, ℓ_p^B and ℓ_p^C, for $N = 10$ (solid lines) and $N = 50$ (dashed lines). Lines and symbols refer to analytical and simulation results, respectively.

uncertainty in the SU position with $\sigma_u = 30\,\mathrm{m}$ and $\sigma_u = 10\,\mathrm{m}$. The results in Fig. 11 highlight similar performance behavior as revealed by the analogous results in the RMSE analysis in Section V-A. Increasing σ_u appears to result in performance degradation in all PU location scenarios. Fig. 11 also demonstrates the effect of reducing σ_u - the curves converge to the case of no-uncertainty.

Path-loss Analysis. In Fig. 12 we show the impact the variation of the path-loss exponent α has on the CDF, in the same scenarios considered for investigating the impact of path-loss on the RMSE in Section V-A. According to Fig. 12, the LEP improves with an increase in α and this is due to the same reasoning outlined in Section V-A, i.e., induction of a node selection strategy. For ℓ_p^A scenario, there is lack of dependency on α as it can be observed from the tightness of the CDF curves. However, for ℓ_p^B scenario, the impact of α is apparent and the estimation is more sensitive to this parameter.

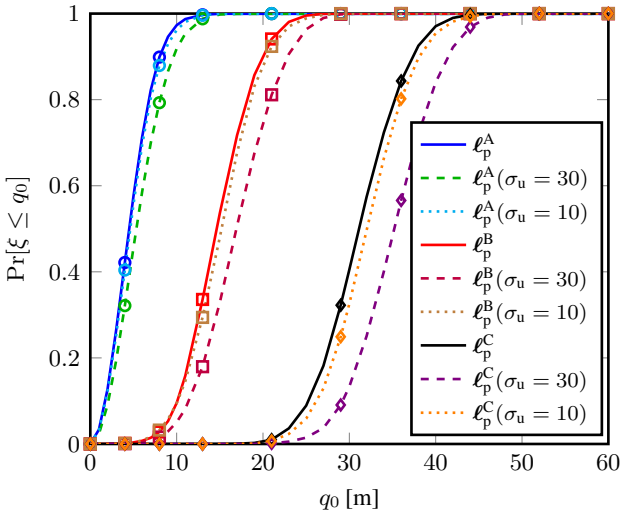

Fig. 11. CDF of the error of the two-dimensional position estimation, in the R-SU case for $N = 50$, when the PU is located at ℓ_p^A, ℓ_p^B and ℓ_p^C, for $\sigma_u = 30\,\mathrm{m}$ and $\sigma_u = 10\,\mathrm{m}$. Dashed curves refer to the RE-SU case when considering uncertainty σ_u. Lines and symbols refer to analytical and simulation results, respectively.

VI. Conclusion

In this paper, we proposed a new analytical framework to calculate the performance of WCL in the presence of i.i.d. and non-i.i.d. log-normal shadowing, based on results on the statistical distribution of the ratio of two quadratic forms in normal variables. In particular, we derived an analytical expression for the RMSE of the two-dimensional location estimation in the presence of non-i.i.d. shadowing, accommodating also the distance-dependent slow-fading intensity. We also provided an analytical expression for the RMSE in the presence of i.i.d. shadowing. The methodology is general enough to include the analysis of the one-dimensional error, which leads also to the calculation of the bias of the position estimate. Such investigation unfolded some peculiarities of WCL which were not known in the literature, e.g., leading to the proposal of a coarse but simple RMSE predictor which only depends on the mean received signal strength, and providing a proof that the position estimate is highly biased. To complete the analysis, a tractable expression for the calculation of the CDF of the localization error is also provided, giving a rather complete statistical description of WCL. The case study analysis confirm that the statistical framework is able to predict the performance of WCL very accurately, capturing all the essential aspects of propagation, SUs location and is well suited for both small and large networks.

References

[1] A. Giorgetti, K. Magowe, and S. Kandeepan, "Exact analysis of weighted centroid localization," in *Proc. European Sig. Pro. Conf. (EUSIPCO)*, vol. 24, Budapest, HUNGARY, August 2016, pp. 743–747.

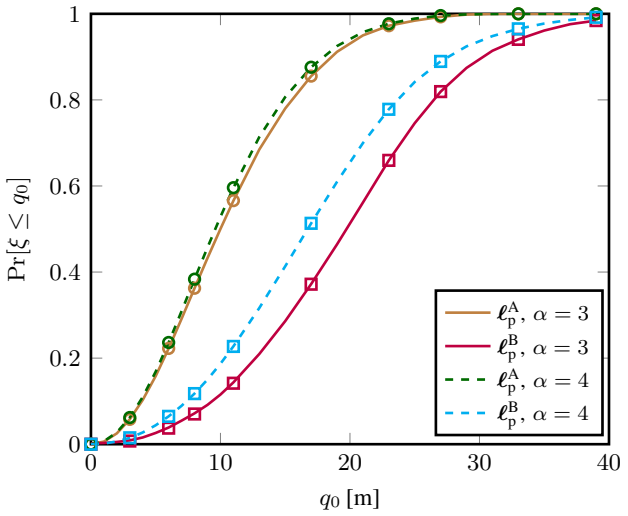

Fig. 12. CDF of the error of the two-dimensional position estimation, in the R-SU case, when the PU is located at $\ell_{\mathrm{p}}^{\mathrm{A}}$ and $\ell_{\mathrm{p}}^{\mathrm{B}}$, and for two different values of the path-loss exponent, with $N = 10$. Lines and symbols refer to analytical and simulation results, respectively.

[2] K. Magowe, A. Giorgetti, S. Kandeepan, and X. Yu, "Statistical distribution of position error in weighted centroid localization," in *Proc. IEEE Int. Conf. on Commun.*, Paris, FRANCE, May 2017, pp. 1–5.

[3] I. F. Akyildiz, B. F. Lo, and R. Balakrishnan, "Cooperative spectrum sensing in cognitive radio networks: A survey," *Elsevier Physical Comm.*, vol. 4, no. 1, pp. 40–62, March 2011.

[4] J. Mitola and G. Q. Maguire, "Cognitive radio: making software radios more personal," *IEEE Pers. Comm.*, vol. 6, no. 4, pp. 13–18, August 1999.

[5] K. Sithamparanathan and A. Giorgetti, *Cognitive Radio Techniques: Spectrum Sensing, Interference Mitigation and Localization.* Boston, USA: Artech House Publishers, November 2012.

[6] W. Dai, Y. Shen, and M. Z. Win, "Distributed power allocation for cooperative wireless network localization," *IEEE J. on Sel. Areas in Commun.*, vol. 33, no. 1, pp. 28–40, January 2015.

[7] A. Mariani, S. Kandeepan, and A. Giorgetti, "Periodic spectrum sensing with non-continuous primary user transmissions," *IEEE Trans. on Wireless Comm.*, vol. 14, no. 3, pp. 1636–1649, March 2015.

[8] P. Pawelczak, K. Nolan, L. Doyle, S. W. Oh, and D. Cabric, "Cognitive radio: Ten years of experimentation and development," *IEEE Commun. Mag.*, vol. 49, no. 3, March 2011.

[9] D. Cabric, I. D. O'Donnell, M.-W. Chen, and R. W. Brodersen, "Spectrum sharing radios," *IEEE Circuits and Sys. Mag.*, vol. 6, no. 2, pp. 30–45, July 2006.

[10] D. Cabric, "Addressing feasibility of cognitive radios," *IEEE Sig. Pro. Mag.*, vol. 25, no. 6, November 2008.

[11] S. Yarkan and H. Arslan, "Exploiting location awareness toward improved wireless system design in cognitive radio," *IEEE Commun. Mag.*, vol. 46, no. 1, pp. 128–136, January 2008.

[12] S. Haykin, "Cognitive radio: brain-empowered wireless communications," *IEEE J. Sel. Areas Commun.*, vol. 23, no. 2, pp. 201–220, February 2005.

[13] S. Bartoletti, W. Dai, A. Conti, and M. Z. Win, "A mathematical model for wideband ranging," *IEEE J. Sel. Topics Signal Process.*, vol. 9, no. 2, pp. 216–228, March 2015.

[14] A. Conti, M. Guerra, D. Dardari, N. Decarli, and M. Z. Win, "Network experimentation for cooperative localization," *IEEE J. Sel. Areas Commun.*, vol. 30, no. 2, pp. 467–475, February 2012.

[15] M. Z. Win, A. Conti, S. Mazuelas, Y. Shen, W. M. Gifford, D. Dardari, and M. Chiani, "Network localization and navigation via cooperation," *IEEE Commun. Mag.*, vol. 49, no. 5, pp. 56–62, May 2011.

[16] W. Dai, Y. Shen, and M. Z. Win, "Energy-efficient network navigation algorithms," *IEEE J. Sel. Areas Commun.*, vol. 33, no. 7, pp. 1418–1430, July 2015.

[17] A. Conti, D. Dardari, M. Guerra, L. Mucchi, and M. Z. Win, "Experimental characterization of diversity navigation," *IEEE Syst. J.*, vol. 8, no. 1, pp. 115–124, March 2014.

[18] X. Wang, L. Gao, S. Mao, and S. Pandey, "CSI-based fingerprinting for indoor localization: A deep learning approach," *IEEE Trans. on Vehicular Tech.*, vol. 66, no. 1, pp. 763–776, January 2017.

[19] A. Rouhollah, B. Fereidoon, A. Mohammad, and S. Maleki, "Exact solution for elliptic localization in distributed MIMO radar systems," *IEEE Trans. on Vehicular Tech.*, vol. PP, no. 99, pp. 1–1, October 2017.

[20] J. Wang, X. Zhang, Q. Gao, H. Yue, and H. Wang, "Device-free wireless localization and activity recognition: A deep learning approach," *IEEE Trans. on Vehicular Tech.*, vol. 66, no. 7, pp. 6258–6267, July 2017.

[21] S. Cai, W. Liao, C. Luo, M. Li, X. Huang, and P. Li, "CRIL: An efficient online adaptive indoor localization system," *IEEE Trans. on Vehicular Tech.*, vol. 66, no. 5, pp. 4148–4160, May 2017.

[22] K.-F. Ssu, C.-H. Ou, and H. C. Jiau, "Localization with mobile anchor points in wireless sensor networks," *IEEE Trans. on Vehicular Tech.*, vol. 54, no. 3, pp. 1187–1197, May 2005.

[23] K. Zheng, H. Wang, H. Li, W. Xiang, L. Lei, J. Qiao, and X. S. Shen, "Energy-efficient localization and tracking of mobile devices in wireless sensor networks," *IEEE Trans. on Vehicular Tech.*, vol. 66, no. 3, pp. 2714–2726, March 2017.

[24] Y. He, A. Behnad, and X. Wang, "Accuracy analysis of the two-reference-node angle-of-arrival localization system," *IEEE Wireless Commun. Lett.*, vol. 4, no. 3, pp. 329–332, June 2015.

[25] K. Tong, X. Wang, A. Khabbazibasmenj, and A. Dounavis, "Optimum reference node deployment for TOA-based localization," in *Proc. IEEE Int. Conf. on Commun. (ICC)*, London, UK, June 2015, pp. 3252–3256.

[26] ——, "RSS-based localization in obstructed environment with unknown path loss exponent," in *Proc. IEEE Vehicular Tech. Conf. (VTC Fall)*, Vancouver, CANADA, September 2014, pp. 1–5.

[27] Y. Shen, W. Dai, and M. Z. Win, "Power optimization for network localization," *IEEE/ACM Trans. on Netwk.*, vol. 22, no. 4, pp. 1337–1350, August 2014.

[28] M. Laghate and D. Cabric, "Cooperatively learning footprints of multiple incumbent transmitters by using cognitive radio networks," *IEEE Trans. on Cogn. Commun. and Netw.*, vol. 3, September 2017.

[29] J. Goodman, K. Rudd, and T. Clancy, "Blind multiuser localization in cognitive radio networks," *IEEE Commun. Lett.*, vol. 16, no. 7, pp. 1018–1021, July 2012.

[30] A. Al-Hourani, R. J. Evans, S. Kandeepan, B. Moran, and H. Eltom, "Stochastic geometry methods for modeling automotive radar interference," *IEEE Trans. on Intelligent Transportation Sys.*, vol. PP, no. 99, pp. 1–12, January 2017.

[31] N. Hettiarachi, S. Kandeepan, and R. Evans, "Automobile radar co-channel interference modeling, simulation and outage analysis," in *Proc. IEEE Int. Conf. on Info. and Commun. Tech. (ICOICT)*, Melaka, MALAYSIA, May 2017, pp. 1–6.

[32] J. Hasch, "Driving towards 2020: Automotive radar technology trends," in *Proc. IEEE Int. Conf. on Microwaves for Int. Mobil. (ICMIM)*, Heidelberg, GERMANY, April 2015, pp. 1–4.

[33] R. Karlsson and F. Gustafsson, "The future of automotive localization algorithms: Available, reliable, and scalable localization: Anywhere and anytime," *IEEE Signal Proc. Mag.*, vol. 34, no. 2, pp. 60–69, March 2017.

[34] S. Bartoletti, A. Conti, and M. Z. Win, "Device-free counting via wideband signals," *IEEE J. on Sel. Areas in Commun.*, vol. 35, no. 5, pp. 1163–1174, May 2017.

[35] ——, "Towards counting via passive radar using ofdm waveforms," in *Proc. IEEE Int. Conf. on Commun. Workshops (ICC Wkshps)*, Paris, FRANCE, May 2017, pp. 803–808.

[36] Y. Shen, S. Mazuelas, and M. Z. Win, "Network navigation: Theory and interpretation," *IEEE J. on Sel. Areas in Commun.*, vol. 30, no. 9, pp. 1823–1834, October 2012.

[37] Y. Shen and M. Z. Win, "On the accuracy of localization systems using wideband antenna arrays," *IEEE Trans. on Commun.*, vol. 58, no. 1, January 2010.

[38] ——, "Fundamental limits of wideband localizationpart I: A general framework," *IEEE Trans. on Inf. Theory*, vol. 56, no. 10, pp. 4956–4980, October 2010.

[39] S. Lee, C. Park, M. J. Lee, and S. Kim, "Multihop range-free localization with approximate shortest path in anisotropic wireless sensor networks," *EURASIP J. on Wireless Commun. and Netwk.*, vol. 2014, no. 1, p. 80, December 2014.

[40] S. Lee, M. Jin, B. Koo, C. Sin, and S. Kim, "Pascal's triangle-based range-free localization for anisotropic wireless networks," *SPRINGER, Wireless Networks*, vol. 22, no. 7, pp. 2221–2238, October 2016.

[41] S. Mazuelas, Y. Shen, and M. Z. Win, "Belief condensation filtering," *IEEE Trans. on Sig. Pro.*, vol. 61, no. 18, pp. 4403–4415, September 2013.

[42] J. Werner, J. Wang, A. Hakkarainen, D. Cabric, and M. Valkama, "Performance and cramer–rao bounds for doa/rss estimation and transmitter localization using sectorized antennas," *IEEE Trans. on Veh. Tech.*, vol. 65, no. 5, pp. 3255–3270, May 2016.
[43] J. Werner, J. Wang, A. Hakkarainen, N. Gulati, D. Patron, D. Pfeil, K. Dandekar, D. Cabric, and M. Valkama, "Sectorized antenna-based doa estimation and localization: Advanced algorithms and measurements," *IEEE J. on Sel. Areas in Commun.*, vol. 33, no. 11, pp. 2272–2286, November 2015.
[44] J. Wang, J. Werner, M. Valkama, and D. Cabric, "Performance analysis of primary user rss/doa estimation and localization in cognitive radio networks using sectorized antennas," *IEEE Wireless Commun. Lett.*, vol. 3, no. 2, pp. 237–240, April 2014.
[45] A. Mariani, S. Kandeepan, A. Giorgetti, and M. Chiani, "Cooperative weighted centroid localization for cognitive radio networks," in *Proc. IEEE Int. Symp. on Comm. and Info. Tech. (ISCIT)*, Gold Coast, AUSTRALIA, October 2012, pp. 459–464.
[46] N. Bulusu, J. Heidemann, and D. Estrin, "GPS-less low-cost outdoor localization for very small devices," *IEEE Personal Commun. Mag.*, vol. 7, no. 5, pp. 28–34, October 2000.
[47] F. Reichenbach and D. Timmermann, "Indoor localization with low complexity in wireless sensor networks," in *Proc. IEEE Int. Conf. on Industrial Informatics*, vol. 4, Singapore, SINGAPORE, August 2006, pp. 1018–1023.
[48] J. Blumenthal, R. Grossmann, F. Golatowski, and D. Timmermann, "Weighted centroid localization in zigbee-based sensor networks," in *Proc. IEEE Int. Symp. on Intelligent Signal Proc. (WISP)*, vol. 5, Alcala de Henares, SPAIN, October 2007, pp. 1–6.
[49] R. Behnke and D. Timmermann, "AWCL: adaptive weighted centroid localization as an efficient improvement of coarse grained localization," in *Proc. IEEE Workshop on Pos., Nav. and Comm. (WPNC)*, vol. 5, Hannover, GERMANY, March 2008, pp. 243–250.
[50] C. Laurendeau and M. Barbeau, "Centroid localization of uncooperative nodes in wireless networks using a relative span weighting method," *EURASIP J. on Wireless Comm. and Netw.*, vol. 2010, pp. 1–10, November 2009.
[51] Y. Chen, Q. Pan, Y. Liang, and Z. Hu, "AWCL: adaptive weighted centroid target localization algorithm based on RSSI in WSN," in *Proc. IEEE Int. Conf. on Comp. Sci. and Info. Tech. (ICCSIT)*, vol. 9, Chengdu, CHINA, July 2010, pp. 331–336.
[52] P. Pivato, L. Palopoli, and D. Petri, "Accuracy of RSS-based centroid localization algorithms in an indoor environment," *IEEE Trans. Instrum. Meas.*, vol. 60, no. 10, pp. 3451–3460, October 2011.
[53] J. Wang, P. Urriza, Y. Han, and D. Cabric, "Weighted centroid localization algorithm: theoretical analysis and distributed implementation," *IEEE Trans. Wireless Commun.*, vol. 10, no. 10, pp. 3403–3413, October 2011.
[54] K. Magowe and S. Kandeepan, "Cooperative blind localization of primary user in a cognitive radio environment," in *Proc. IEEE Int. Conf. on Sig. Proc. and Comm. Sys. (ICSPCS)*, Gold Coast, AUSTRALIA, December 2014, pp. 1–8.
[55] A. Fink and H. Beikirch, "Refinement of weighted centroid localization using a regular infrastructure topology," in *Proc. IEEE Int. Conf. on Indoor Pos. and Indoor Nav. (IPIN)*, Busan, KOREA, October 2014, pp. 501–510.
[56] K. Magowe, S. Kandeepan, A. Giorgetti, and X. Yu, "Constrained cluster based blind localization of primary user for cognitive radio networks," in *Proc. IEEE Int. Symp. on Personal, Indoor, and Mobile Radio Comm. (PIMRC)*, Hong Kong, CHINA, September 2015, pp. 986–991.
[57] A. Razavi, M. Valkama, and E.-S. Lohan, "K-means fingerprint clustering for low-complexity floor estimation in indoor mobile localization," in *Proc. IEEE Global Comm. Conf. Workshops (Globecom Wkshps)*, San Diego, USA, December 2015, pp. 1–7.
[58] N. Saeed and H. Nam, "Robust multidimensional scaling for cognitive radio network localization," *IEEE Trans. Veh. Technol.*, vol. 64, no. 9, pp. 4056–4062, September 2015.
[59] S. Chaudhari and D. Cabric, "Cyclic weighted centroid algorithm for transmitter localization in the presence of interference," *IEEE Trans. on Cogn. Commun. Netw.*, vol. 2, no. 2, pp. 162–177, June 2016.
[60] A. Ullah, *Finite sample econometrics*. Oxford University Press, 2004.
[61] Y. Bao and R. Kan, "On the moments of ratios of quadratic forms in normal random variables," *ELSEVIER J. of Multivariate Analysis*, vol. 117, pp. 229–245, January 2015.
[62] S. Chaudhari and D. Cabric, "Cyclic weighted centroid localization for spectrally overlapped sources in cognitive radio networks," in *Proc. IEEE Global Commun. Conf. (GLOBECOM)*, Austin, USA, December 2014, pp. 935–940.
[63] J. R. Magnus, "The exact moments of a ratio of quadratic forms in normal variables," *JSTOR Annales d'Economie et de Statistique*, pp. 95–109, October 1986.
[64] J. Sherman and W. J. Morrison, "Adjustment of an inverse matrix corresponding to changes in the elements of a given column or a given row of the original matrix," *JSTOR Annals of Mathematical Statistics*, vol. 20, no. 4, pp. 621–621, December 1949.
[65] J. Imhof, "Computing the distribution of quadratic forms in normal variables," *JSTOR Biometrika*, vol. 48, no. 3/4, pp. 419–426, December 1961.
[66] J. Gil-Pelaez, "Note on the inversion theorem," *Biometrika*, vol. 38, no. 3-4, pp. 481–482, December 1951.
[67] M. Gudmundson, "Correlation model for shadow fading in mobile radio systems," *Electron. Lett.*, vol. 27, no. 23, pp. 2145–2146, November 1991.
[68] D. Giancristofaro, "Correlation model for shadow fading in mobile radio channels," *Electron. Lett.*, vol. 32, no. 11, pp. 958–959, February 1996.
[69] H. Claussen, "Efficient modelling of channel maps with correlated shadow fading in mobile radio systems," in *Proc. IEEE Int. Symp. on Personal, Indoor, and Mobile Radio Comm. (PIMRC)*, vol. 4, Berlin, GERMANY, September 2005, pp. 512–516.
[70] A. F. Molisch, Z. Hijaz, W. J. Nunan, and L. F. Zapanta, "On pathloss models for adjacent-channel interference in cognitive whitespace systems," in *Proc. IEEE Int. Conf. on Comm. Workshops (ICC Wkshps)*, Kuala Lumpur, MALAYSIA, May 2016, pp. 682–688.

Kagiso Magowe (S'10–M'18) received B.Eng. (Hons) and M.Eng. (by Research) degrees in telecommunications engineering from the University of South Australia, Adelaide, Australia, in 2010 and 2012, respectively. He received the Ph.D. degree in electronics and telecommunications engineering from RMIT University, Melbourne, Australia, in 2017. He is currently a Research Fellow with the School of Engineering, RMIT University. His research interests include communication theory, information theory, statistical signal processing, application of linear algebra, cognitive radios, and localization. Dr. Magowe was the recipient of the Codan Achievement Prize in Telecommunications in 2009 (Codan Limited), University President Scholarship in 2010 (University of South Australia), and the Australian Postgraduate Award funded by the Australian government in 2014 (RMIT University).

Andrea Giorgetti (S'98–M'04–SM'13) received the Dr. Ing. degree (*summa cum laude*) in electronic engineering and the Ph.D. degree in electronic engineering and computer science from the University of Bologna, Italy, in 1999 and 2003, respectively. From 2003 to 2005, he was a Researcher with the National Research Council, Italy. He joined the Department of Electrical, Electronic, and Information Engineering "Guglielmo Marconi," University of Bologna, as an Assistant Professor in 2006 and was promoted to Associate Professor in 2014. In spring 2006, he was with the Laboratory for Information and Decision Systems (LIDS), Massachusetts Institute of Technology (MIT), Cambridge, MA, USA. Since then, he has been a frequent visitor to the Wireless Information and Network Sciences Laboratory at the MIT, where he presently holds the Research Affiliate appointment.

His research interests include ultrawide bandwidth communication systems, active and passive localization, wireless sensor networks, and cognitive radio. He has co-authored the book *Cognitive Radio Techniques: Spectrum Sensing, Interference Mitigation, and Localization* (Artech House, 2012). He was the Technical Program Co-Chair of several symposia at the IEEE Int. Conf. on Commun. (ICC), and IEEE Global Commun. Conf. (Globecom). He has been an Editor for the IEEE COMMUNICATIONS LETTERS and for the IEEE TRANSACTIONS ON WIRELESS COMMUNICATIONS. He has been elected Chair of the IEEE Communications Society's Radio Communications Technical Committee.

Sithamparanathan Kandeepan (SM09) received the Ph.D. degree from the University of Technology Sydney, Sydney. He was with the NICTA Research Laboratory, Canberra, and with the CREATE-NET Research Center, Italy. He is currently an Associate Professor with the School of Engineering, RMIT University. He has authored more than one hundred peer reviewed journals and conference papers, including a scholarly book with Dr. A. Giorgetti entitled Cognitive Radio Techniques: Spectrum Sensing, Interference Mitigation, and Localization. He had received an IEEE Exemplary Reviewer award in 2011, and a Certificate of Appreciation in 2015 for 10 years of contributions to the field from the IEEE Communications Society. He had served as a Vice Chair of the IEEE Technical Committee on Cognitive Networks, and currently serves as the Chair of the IEEE VIC region Communications Society Chapter. He was the Chair of several IEEE Workshops in several conferences, such as the ICC, the GLOBECOM, and the VTC. He serves as the Editor for the special issue in the ETT-Wiley journal on Future Evolution of Public Safety Communications in the 5G Era. His research interests are on cognitive radios, statistical performance analysis, and the development of signal processing techniques.

Xinghuo Yu (M'92–SM'98–F'08) received BEng and MEng degrees in Electrical and Electronic Engineering from the University of Science and Technology of China, Hefei, China, in 1982 and 1984, and PhD degree in Control Science and Engineering from Southeast University, Nanjing, China in 1988, respectively. He is an Associate Deputy Vice-Chancellor and a Distinguished Professor at RMIT University (Royal Melbourne Institute of Technology), Melbourne, Australia. He is also the President of IEEE Industrial Electronics Society for 2018 and 2019. His research interests include control systems, complex and intelligent systems, and smart grids. He received a number of awards and honors for his contributions, including 2013 Dr.-Ing. Eugene Mittelmann Achievement Award of IEEE Industrial Electronics Society and 2018 M. A. Sargent Medal of Engineers Australia. He has been named a Highly Cited Researcher by Clarivate Analytics (formerly Thomson Reuters) since 2015.